A New Plasma Jet Array Source: Discharge Characteristics and Mechanism

Dong Li, Dingxin Liu, *Member, IEEE*, Zeyu Chen, Mingzhe Rong, *Senior Member, IEEE*, and Michael G. Kong, *Fellow, IEEE*

***Abstract*— A new plasma jet array source is reported, which has two plasma regions: a cylindrical bottle in which plasmas are generated to deposit charged species on the inner wall, and the outside atmosphere in which plasma jets are generated between the small holes in the underside of the bottle and the grounded sample underneath the bottle. Four temporal regions of discharge are found to exist during a voltage cycle, in which the first one has maximal amount of charge transfer but minimal discharge energy. The surface charges supply the seed charge to initiate and sustain the plasma jets, while restricting the intensity of each plasma jet because their amount is limited. Only the surface charges near the underside hole of the cylindrical bottle are possible to participate in the discharge. Therefore, the plasma jets have a good jet-to-jet homogeneity relatively independent of the number of jets and their relative positions, indicating that the plasma jets can be arbitrarily arranged to a large extent. This is an application advantage but with a limitation, i.e., two plasma jets cannot be closer than 2.5 mm, because the surface charge between them will be shunted, and therefore, the plasma jets will be weakened.**

***Index Terms*— Homogeneity, plasma jet array, surface charge.**

I. Introduction

COLD atmospheric-pressure plasmas have attracted many interests for diverse application fields, such as material modification [1] and biomedical application [2]–[4] in the last decade. Plasma jet is one of the most common sources for producing cold atmospheric-pressure plasmas, which normally consists of a dielectric tube with gas flow in it, a high-voltage electrode surrounding or inner the tube, and a grounded electrode separated from the high-voltage electrode by the tube wall or by a certain distance in open air [5]. The grounded electrode is sometimes not necessary, because the open air or the treated sample in the downstream region of the plasma jet can act as the virtual ground [5]. Plasma jet has an advantage of blowing a plasma plume into open air, and therefore, the sample to be treated is no longer restricted by the narrow discharge gap, which is normally in millimeter scale. However, the plasma plume has a cross section comparable with the inner section of the tube, commonly in square millimeters. This cross section corresponds to the plasma treatment area, which is too small to meet the requirement of many applications [5], [6]. Therefore, plasma jet arrays have been developed with the combination of several to several tens of plasma jet sources, and consequently, a large area can be treated by the plasmas simultaneously [6]–[9].

Several different structures have been reported for the sources of plasma jet arrays, but most of them have similar principles in essence, i.e., plasma jet sources are in parallel in a circuit and the plasmas are generated simultaneously when a high voltage is applied [6]–[9]. Tiny difference among the sources may result in big inhomogeneity among the plasma jets, and consequently, ballast resistances are usually used to reduce the influence of such difference, but on the other hand, a part of electrical energy is lost by Joule heating of the ballast resistance [7], [10]. Some jet array sources have good jet-to-jet homogeneity without using the ballast resistances [11], but the sources must be made very carefully. Because the plasma jets are easy to be inhomogeneous, a plasma jet array source is relatively difficult to be made, and it is even difficult to make some change on a manufactured source to meet different requirements, such as change the jet positions.

In this paper, a new plasma jet array source is reported. It has two plasma regions: a cylindrical bottle in which plasmas are generated to deposit charged species on the inner wall, and the outside atmosphere in which plasma jets are initiated by the surface charges through small holes in the underside of the bottle. The surface charges also act as the limiter of each plasma jet, since their amount is limited on a certain area around a hole. The jet positions can be changed as well with good jet-to-jet homogeneity, unless two jets are too close to have strong interaction between each other. The structure of the plasma jet array source, the discharge characteristics, and the control of the jet positions will be presented in the following, which are much different to the existing plasma jet arrays that are reported in the literature.

II. Experimental Setup

Fig. 1(a) shows the schematic of the experimental setup for two plasma jets. Helium gas (purity 99.999%) flows through a cylindrical stainless steel tube of 3.8 mm inner diameter and 4 mm outer diameter, and the flow rate is 1.5 L/min.

Manuscript received January 30, 2016; revised August 18, 2016; accepted September 2, 2016. Date of publication October 19, 2016; date of current version November 7, 2016. This work was supported in part by the National Science Foundation of China under Grant 51521065, in part by the Fundamental Research Funds for the Central Universities, and in part by the State Key Laboratory of Electrical Insulation and Power Equipment under Grant EIPE14123. *(Corresponding author: Dingxin Liu.)*

D. Li, D. Liu, Z. Chen, and M. Rong are with the State Key Laboratory of Electrical Insulation and Power Equipment, Xi'an Jiaotong University, Xi'an 710049, China (e-mail: liudingxin@mail.xjtu.edu.cn).

M. G. Kong is with the State Key Laboratory of Electrical Insulation and Power Equipment, Xi'an Jiaotong University, Xi'an 710049, China, and also with the Frank Reidy Center for Bioelectrics, Old Dominion University, Norfolk, VA 23508 USA.

Color versions of one or more of the figures in this paper are available online at http://ieeexplore.ieee.org.

Digital Object Identifier 10.1109/TPS.2016.2612261

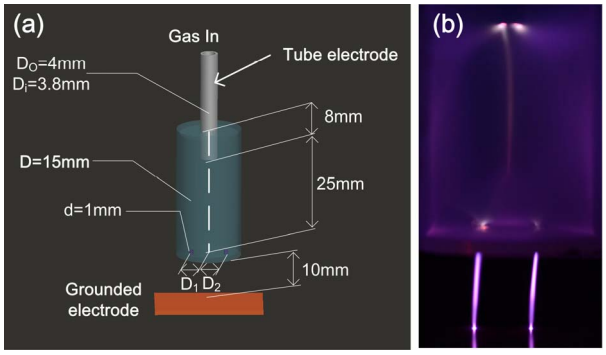

Fig. 1. (a) Schematic of the plasma jet array source and (b) photograph of the plasmas for the peak-to-peak applied voltage of 8.5 kV and the helium flow rate of 1.5 slm. The center distance of the holes is $D1 = D2 = 2$ mm.

The tube insets in a cylindrical bottle at the center point of its top surface, which is the high-voltage electrode of the plasma jet array source. The bottle is made of polypropylene with a height of 33 mm and an inner diameter of 15 mm. The distance from the end of the tube to the underside of the bottle is 25 mm. Two holes of 1 mm diameter are located symmetrically in the underside, and the center distance of each hole is 2 mm. The helium gas inside the bottle can flowthrough the holes to the outside atmosphere. A grounded plane electrode is located 10 mm away from the underside of the bottle. The applied voltage has a peak-to-peak value of 8.5 kV and a frequency of 20 kHz. The discharge image with an exposure time of 1 s is obtained by a digital camera (Nikon, D7000), as shown in Fig. 1(b). In the bottle, plasma is generated which seems to fill the whole inner space, although a more luminous channel is formed along the axis. In addition, two plasma jets are generated between the holes in the underside of the bottle and the downstream grounded electrode with relatively similar intensity.

The applied voltage is measured with a high-voltage probe (Tektronix, P6015A), and the discharge current through both the high-voltage electrode (I_{HV}) and the grounded electrode (I_G) is measured by two current probes (Tektronix, P6021). The waveforms of discharge voltage and current are recorded by an oscilloscope (Tektronix, DPO3000). The conduction current is obtained by subtracting the displacement current from the discharge current, and the displacement current is measured for the same jet array source but without the helium gas flow, i.e., no discharge is observed. As will be presented in the following, the waveforms of the conduction currents through the high-voltage electrode (I_{HV}) and the grounded electrode (I_G) are much different. The amount of charge transfer is obtained by integrating the conduction current with time. To study the dynamic evolution of the discharge, an intensified charge-coupled device (iCCD) camera (Princeton Instrument, PI Max-3) is used. In addition, the emission spectra of the plasmas inside and outside the bottle are measured by a spectrometer (Ocean Optics, USB2000).

III. Experimental Results

The waveforms of discharge voltage and conduction current through the high-voltage electrode (I_{HV}, green line) and the grounded electrode (I_G, red line) are shown in Fig. 2(a).

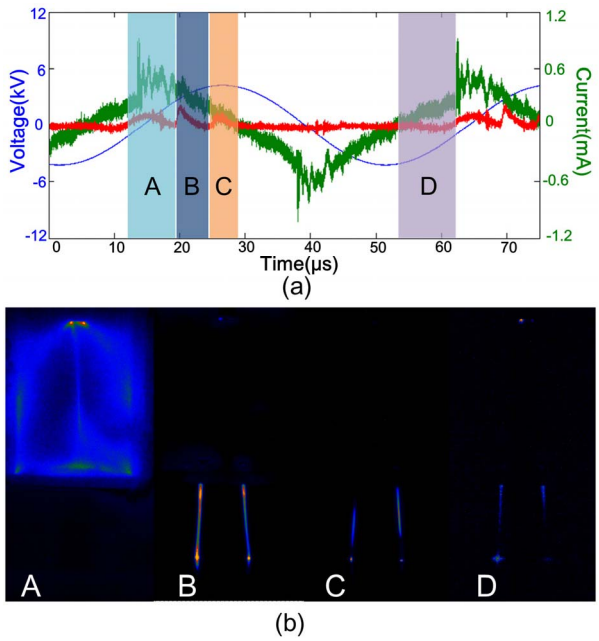

Fig. 2. (a) Waveforms of discharge voltage and conduction current. (b) Discharge images corresponding to the temporal regions marked with A–D.

The waveform of I_{HV} is in general symmetric in the positive and negative half-cycle, but it has several random pulses in each half cycle. From the waveform of I_G, there are three discharge pulses (temporal regions A–C) in the positive half-cycle of the applied voltage and one (region D) in the negative half-cycle. The current pulse widths are 7.8, 5.3, 3.3, and 8.7 μs for the four temporal regions, respectively. Four discharges happen in one cycle of the applied voltage, which correspond to the pulses of I_G. The discharge images are shown in Fig. 2(b), which are taken by the iCCD with the exposure times corresponding to the temporal regions A–D.

In the temporal region A, the plasma is mainly confined in the cylindrical bottle, which fills the inner space of the bottle and deposits charged species on the inner wall. In the other temporal regions (B–D), two plasma jets happen between the holes in the underside of the bottle and its downstream grounded electrode, but the plasma in the bottle is very weak. In general, this indicates that the discharges inside and outside the cylindrical bottle do not happen in the same time, and they have much different features. This also explains the difference between the waveforms of I_{HV} and I_G, as shown in Fig. 2(a). The amounts of charge transfer are found to be 0.44, 0.29, and 0.16 nC for the three positive pulses and -0.12 nC for the negative pulse of I_G, i.e., the charge transfer peaks in the first discharge. However, the average discharge powers for these four temporal regions are 0.03, 0.23, 0.19, and 0.04 W, respectively, and hence, the discharge power minimizes in the first discharge. The first discharge has maximal amount of charge transfer but minimal discharge energy, suggesting that it is a prebreakdown process for the plasma jets outside the cylindrical bottle. This prebreakdown process deposits surface charges that initiate the subsequent plasma jets (will be further discussed in the following). As shown in Fig. 2(a), the absolute value of I_{HV} is much higher than that of I_G in both the positive

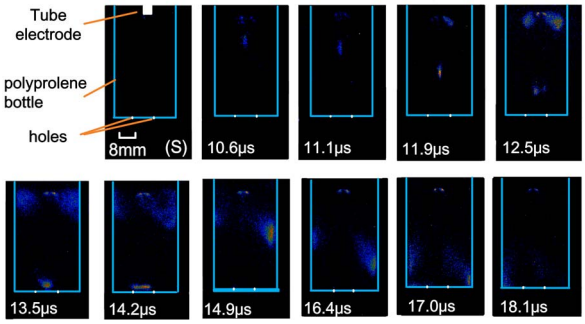

Fig. 3. Discharge structure in the polyprolene bottle (S) and the evolution of discharge images in different times within temporal region A.

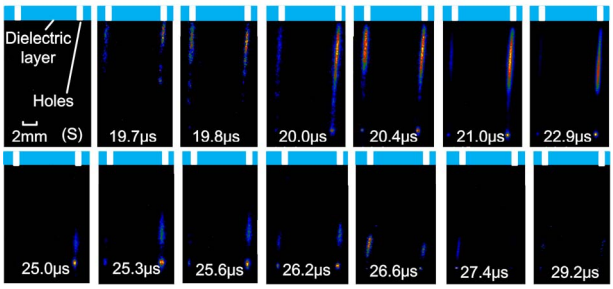

Fig. 4. Discharge structure outside the polyprolene bottle (S) and the evolution of discharge images in different times within temporal regions B and C.

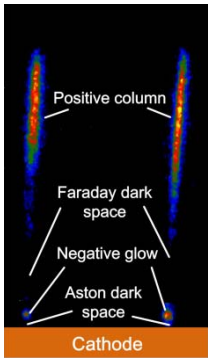

Fig. 5. Typical image of the discharge in temporal region B.

and negative voltage half-cycles, implying that only a small part of the surface charges supplied by I_{HV} is consumed by the plasma jets (pulses of I_G) outside the cylindrical bottle. A comparatively larger amount of them transfer back to the tube electrode as the voltage reverses. The prebreakdown process consumes just ~6% of the total input power, indicating that the discharge voltage in the bottle should be much lower than that outside it. This should be attributed to the different working gases in both regions, i.e., helium dominates in the bottle, but air dominates outside it.

In order to further investigate the discharge process, the iCCD camera is used to capture the images with an exposure time of 10 ns. The evolution of discharge images in the temporal region A is shown in Fig. 3, from which it can be seen that the plasma initiates at the high-voltage tube electrode which located near the top surface of the cylindrical bottle, and then, it propagates to the inner wall of the bottle through three branches: one propagates directly to the underside, and the other two first propagate to the side wall and then to the underside. The central branch of the plasma looks like a plasma bullet [5], which propagates fastest with an average velocity of $\sim 5 \times 10^4$ m/s, and it reaches the underside of the bottle at the instant of 12.8 μs [the instant values in the subfigures corresponds to that in Fig. 2(a)]. The velocity is obtained by dividing the front position of the central plasma branch by time, which is in the typical range of plasma bullet at 10^3 ~10^6 m/s in the open air [5], [11], [12].

After arriving at the underside, the bullet-like plasma flattens and expands on the surface of the underside till the two holes (see the subfigures at 13.5 and 14.2 μs). The other two branches of the plasma arrive at the sidewall at the instant of ~13 μs, and then, they propagate downward to reach the underside at the instant of ~17 μs; finally, they disappear when arriving that the two holes. The evolution process of the first discharge in the cylindrical bottle shows clearly that it provides the seed charge for the subsequent plasma jets.

The evolution of discharge images in the temporal regions B and C is shown in Fig. 4. A large amount of surface charge have been deposited on the underside of the bottle after the temporal region A, and hence, such underside has high positive potential to the underneath grounded electrode. This makes the underside of the bottle play as the virtual anode in the temporal region B, and the plasma jets initiate at the holes of the underside, because the surface charge provides seed charges there. The plasma jets propagate to the downstream grounded electrode and reach there at the instant of ~20 μs, and they sustain for about 3 μs before quenching. Approximately 1 μs after that, the third discharge occurs which corresponds to temporal region C. The third discharge is comparatively weaker, and it seems like to propagate from the grounded electrode to the holes in the underside of the bottle. No surface charge is accumulated on the grounded electrode to initiate the third discharge, so it may be a restrike of the prior one, because the discharge channels do not recover completely.

A closer look at the plasma structure of the plasma plume at 20.4 μs is shown in Fig. 5. It can be seen that the discharge has the glow discharge structure, including the Aston dark space, negative glow, Faraday dark space, and positive column. This pattern has also been reported in some studies for kilohertz excited atmospheric discharges [13], [14].

On contrast, there is a unique discharge pulse in the negative half cycle, and the plasmas exist both in the cylindrical bottle and outside atmosphere at the same time, as shown in Fig. 2. The last discharge is even weaker and hence not discusses more in this paper.

In order to further characterize the discharges inside and outside the polypropylene bottle, the optical emission spectra of them are also measured, as shown in Fig. 6. It can be seen that the emission intensities of N_2^+(B), He*, and O($3p^5P$) dominate in the bottle, while the emission intensities of NO(A), OH(A), and N_2(C) dominate in the open air. The relationship of emission intensities corresponds to that of the species densities. In the open air, the emission lines of helium metastables are not observed, suggesting that the helium concentration in the air gap is low. This indicates that the glow discharge (see Fig. 5) happens in the air-dominated working gas, which is not easy to be realized. The potential energy

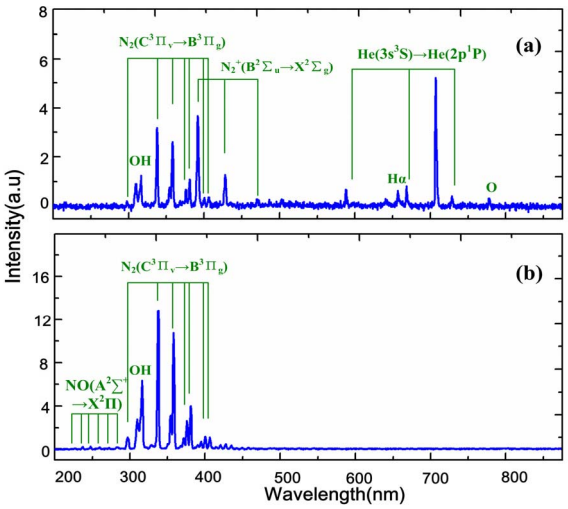

Fig. 6. Emission spectra of the discharges in (a) cylindrical bottle and (b) downstream open air.

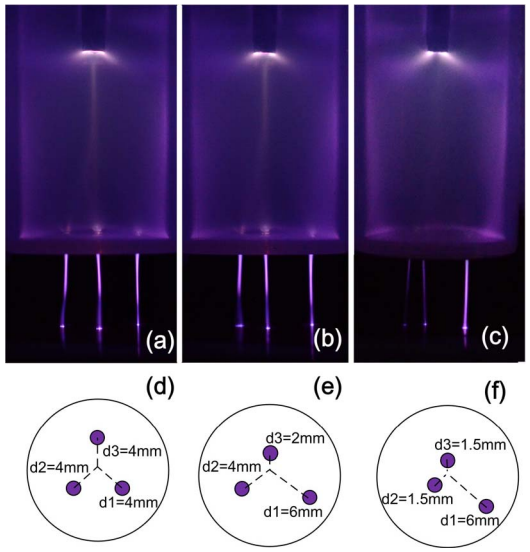

Fig. 7. (a)–(c) Discharge photographs for different position distributions of holes in the underside of the cylindrical bottle. (d)–(f) End views of the position distributions of holes.

of NO(A) state is 5.5 eV, which can be excited by collision with He^* or $N_2(C)$ (excitation energy of 11.1 eV) [15]. The NO excitation cross section by collision with $N_2(C)$ is much higher than that for He^*, and hence, NO(A) has higher density in the open air [15]. The higher density of OH(A) may be attributed to the higher density of water vapor in the open air. As for the $O(3p^5P)$, the main chemical pathways for $O(3p^5P)$ in $He+O_2$ cold atmospheric-pressure plasmas are listed in the following [16]:

$$e + O_2 \rightarrow O(3p^5P) + O + e \quad (1)$$

$$He^* + O_2 \rightarrow O(3p^5P) + O + He \quad (2)$$

$$He_2^* + O_2 \rightarrow O(3p^5P) + O + 2He \quad (3)$$

$$O(3p^5P) + He \rightarrow O + He \quad (4)$$

$$O(3p^5P) + O_2 \rightarrow O + O_2. \quad (5)$$

It means that the helium metastables play an important role in the generation of the $O(3p^5P)$. In the outside atmosphere, the density of the helium metastables is comparatively lower, and so does the $O(3p^5P)$ density.

It is also worth noting that these reactive species are useful for medical treatment. For example, it has been reported that the NO has a dramatically positive influence on the wound healing process [17]. OH is widely used for sterilization, and it is also reported to have a beneficial effect on cancer treatment [18], [20].

As mentioned earlier, the plasma jets are initiated by the surface charge, so the position of a hole may be important for the corresponding plasma jet. From the application point of view, the jet-to-jet homogeneity is crucial for a plasma jet array source, and hence, it is essential to check the influence of the hole positions on the plasma jet homogeneity. For this purpose, three position distributions of holes in the underside are investigated, and each underside has three holes, as shown in Fig. 7(d)–(f). Their discharge images are shown in Fig. 7(a)–(c), respectively. The discharge images are also taken by a digital camera (Nikon, D7000) with the exposure time of 1 s. As shown in Fig. 7(a) and (b), the plasma jets have a good jet-to-jet homogeneity, and we note that each jet has similar intensity to that with two holes in the underside. This suggests that each plasma jet is relatively independent of the number of holes and their position distributions. In principle, only the surface charges near a hole are possible to participate in the plasma jet, which ignite the plasma jet but on the other hand restrict the plasma intensity because their amount is limited. This may be the reason for the independence of each plasma jet. For the potential applications, it is an advantage, because the positions that to be treated can be easily controlled by changing the corresponding positions of the holes.

This application advantage has a limitation, i.e., the plasma jets can be influence when two holes are too closer. As shown in Fig. 7(c), the plasma jets are obviously weakened when the distance of the two holes is 2.5 mm. This indicates that the distance between two holes has a critical value under which the jet arrays would no longer homogeneous, which may be attributed to surface charge between the two holes that are shunted by the plasma jets. This critical distance between two holes should be dependent on many factors, such as the permittivity of the bottle material, the shape of the bottle, the applied voltage, and so on.

IV. Conclusion

In summary, a new plasma jet array source is reported which has two plasma regions: a cylindrical bottle in which plasmas are generated to deposit charged species on the inner wall, and the outside atmosphere in which plasma jets are generated between the small holes in the underside of the bottle and the grounded sample underneath the bottle. Four temporal regions of discharge are found to exist during a voltage cycle. In the first one, the plasma initiates at the tube electrode which located at the top of the cylindrical bottle, and it propagates to the inner wall of the bottle through three branches: one propagates directly to the underside, and the other two first propagate to the side wall and then to the underside.

The plasma is confined in the cylindrical bottle. In the second one, the plasma jets initiate at the holes in the underside of the bottle, and they propagate toward the underneath grounded electrode. Each plasma jet has the typical structure of a glow discharge although the open air is strongly diluted in the working gas (helium gas flow is relatively low). The third discharge is similar to the second one only its intensity is weaker, and the last discharge occurs in the negative half-cycle of the applied voltage. Compared with the four temporal regions, the first one has maximal amount of charge transfer but minimal discharge energy, suggesting that it plays as a good charge supplier for the subsequent plasma jets, and the energy efficiency of the plasma jets is high, because they consumes ∼94% of the total energy.

The surface charges supply the seed charge to initiate and sustain the plasma jets, while restricting the intensity of each plasma jet because their amount is limited. Only the surface charges near to the underside hole of the cylindrical bottle are possible to participate in the discharge. Therefore, the plasma jets have a good jet-to-jet homogeneity relatively independent of the number of jets and their relative positions, indicating that the plasma jets can be arbitrarily arranged to a large extent. This is an application advantage but with a limitation, i.e., two plasma jets cannot be closer than 2.5 mm because the surface charge between them will be shunted, and therefore, the plasma jets will be weakened.

REFERENCES

[1] K. G. Kostov, T. M. C. Nishime, A. H. R. Castro, A. Toth, and L. R. O. Hein, "Surface modification of polymeric materials by cold atmospheric plasma jet," *Appl. Surf. Sci.*, vol. 314, pp. 367–375, Sep. 2014.

[2] M. G. Kong *et al.*, "Plasma medicine: An introductory review," *New J. Phys.*, vol. 11, no. 11, p. 115012, 2009.

[3] N. Barekzi and M. Laroussi, "Effects of low temperature plasmas on cancer Cells," *Plasma Process. Polym.*, vol. 10, no. 12, pp. 1039–1050, 2013.

[4] M. Laroussi, "Low-temperature plasmas for medicine?" *IEEE Trans. Plasma Sci.*, vol. 37, no. 6, pp. 714–725, Jun. 2009.

[5] X. Lu, G. V. Naidis, M. Laroussi, and K. Ostrikov, "Guided ionization waves: Theory and experiments," *Phys. Rep.*, vol. 540, no. 3, pp. 123–166, 2014.

[6] M. Ghasemi, P. Olszewski, J. W. Bradley, and J. L. Walsh, "Interaction of multiple plasma plumes in an atmospheric pressure plasma jet array," *J Phys. D, Appl. Phys.*, vol. 46, no. 5, p. 052001, 2013.

[7] Q. Y. Nie, Z. Cao, C. S. Ren, D. Z. Wang, and M. G. Kong, "A two-dimensional cold atmospheric plasma jet array for uniform treatment of large-area surfaces for plasma medicine," *New J. Phys.*, vol. 11, p. 115015, Nov. 2009.

[8] C. Zhang, T. Shao, Y. X. Zhou, Z. Fang, P. Yan, and W. Yang, "Effect of O_2 additive on spatial uniformity of atmospheric-pressure helium plasma jet array driven by microsecond-duration pulses," *Appl. Phys. Lett.*, vol. 105, no. 4, p. 044102, 2014.

[9] G. Konesky, "Cold plasma decontamination using flexible jet arrays," *Proc. SPIE*, vol. 7665, p. 76651P, May 2010, doi: 10.1117/12.849943.

[10] Z. Cao, J. L. Walsh, and M. G. Kong, "Atmospheric plasma jet array in parallel electric and gas flow fields for three-dimensional surface treatment," *Appl. Phys. Lett.*, vol. 94, no. 2, p. 021501, 2009.

[11] J. Y. Kim, J. Ballato, and S.-O. Kim, "Intense and energetic atmospheric pressure plasma jet arrays," *Plasma Process. Polym.*, vol. 9, no. 3, pp. 253–260, 2012.

[12] J. L. Walsh, P. Olszewski, and J. W. Bradley, "The manipulation of atmospheric pressure dielectric barrier plasma jets," *Plasma Sour. Sci. Technol.*, vol. 21, no. 3, p. 034007, 2012.

[13] S. Wu, H. Xu, X. Lu, and Y. Pan, "Effect of pulse rising time of pulse dc voltage on atmospheric pressure non-equilibrium plasma," *Plasma Process. Polym.*, vol. 10, no. 2, pp. 136–140, 2013.

[14] J. L. Walsh, F. Iza, N. B. Janson, V. J. Law, and M. G. Kong, "Three distinct modes in a cold atmospheric pressure plasma jet," *J. Phys. D, Appl. Phys.*, vol. 43, no. 7, p. 075201, 2010.

[15] N. Gherardi, G. Gouda, E. Gat, A. Ricard, and F. Massines, "Transition from glow silent discharge to micro-discharges in nitrogen gas," *Plasma Sour. Sci. Technol.*, vol. 9, no. 3, pp. 340–346, 2000.

[16] X. Lu and M. Laroussi, "Optimization of ultraviolet emission and chemical species generation from a pulsed dielectric barrier discharge at atmospheric pressure," *J. Appl. Phys.*, vol. 98, no. 2, p. 023301, 2005.

[17] J. L. Walsh, D. X. Liu, F. Iza, M. Z. Rong, and M. G. Kong, "Contrasting characteristics of sub-microsecond pulsed atmospheric air and atmospheric pressure helium–oxygen glow discharges," *J. Phys. D, Appl. Phys.*, vol. 43, no. 3, p. 032001, 2010.

[18] G. Fridman, G. Friedman, A. Gutsol, A. B. Shekhter, V. N. Vasilets, and A. Fridman, "Applied plasma medicine," *Plasma Process. Polym.*, vol. 5, no. 6, pp. 503–533, Aug. 2008.

[19] K. Ninomiya *et al.*, "Evaluation of extra-and intracellular oh radical generation, cancer cell injury, and apoptosis induced by a non-thermal atmospheric-pressure plasma jet," *J. Phys. D, Appl. Phys.*, vol. 46, no. 42, p. 425401, 2013.

[20] D. H. Xu *et al.*, "*In Situ* oh generation from O_2^- and H_2O_2 plays a critical role in plasma-induced cell death," *PLoS ONE*, vol. 10, no. 6, p. e0128205, 2015.

Authors' photographs and biographies not available at the time of publication.